JACS Au
AN OPEN ACCESS JOURNAL OF THE AMERICAN CHEMICAL SOCIETY

pubs.acs.org/jacsau
Article

Toward an Understanding of Linear Scaling Relations through Energy Decomposition Analysis

Jesse DiCenso,[⊥] Chance Lander,[⊥] Zheng Pei, Sanghita Sengupta, Tien Le, Yu Zhang, G. T. Kasun Kalhara Gunasooriya, Bin Wang, Yuezhi Mao,* and Yihan Shao*

Cite This: JACS Au 2025, 5, 3092−3103

Read Online

ACCESS | Metrics & More | Article Recommendations | Supporting Information

ABSTRACT: The discovery of linear scaling relations has fundamentally changed the field of heterogeneous catalysis. The scaling relations have been rationalized based on the d-band theory, specifically a separation of sp and d electron contributions to adsorption energies. Within the framework of energy decomposition analysis, a full understanding of such a separation would require one to further break down the adsorption energy into distinct energy components such as electrostatics, polarization, charge transfer, and van der Waals interactions, and to examine the sp and d contributions to each of them. As a step in this direction, we analyzed the interaction energy between CH_x (x = 1−4) adsorbates and fcc(100) transition metal surfaces (M = Cu, Ag, Au, Rh, and Pt), with the surfaces represented both as slabs in plane-wave density functional theory (pw-DFT) calculations and as atomic clusters in atomic-orbital basis density functional theory (ao-DFT) calculations. Through an absolutely localized molecular orbital (ALMO) based energy decomposition analysis of the ao-DFT adsorption energy, each of the interaction energy components (electrostatics, polarization, van der Waals, and charge transfer) was found to follow its own scaling relations, with an intricate interplay among these energy components yielding the overall scaling relations for the total adsorption energies. Using the recently introduced ALMO-based polarization and charge-transfer analysis schemes, we further dissected polarization into metal surface and adsorbate contributions, and charge transfer into metal → adsorbate and adsorbate → metal contributions. The contributions from the sp and d electrons of the metal to these terms were further quantified, and the dominant role of the metal d electrons was reaffirmed. These results shed light on how CH_x adsorbates interact with metal surfaces and further reveal the physical origin of the scaling relations.

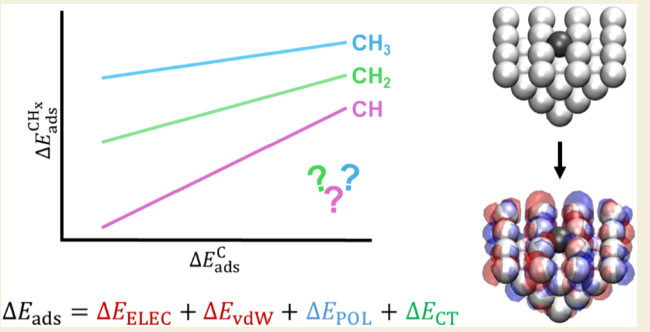

KEYWORDS: *scaling relations, absolutely localized molecular orbitals, energy decomposition, complementary occupied-virtual pair, surface reactions*

1. INTRODUCTION

The adsorption of molecules onto metal surfaces is a fundamental step in the field of heterogeneous catalysis, where metal catalysts facilitate water−gas shift, hydrogenation, isomerization, electrocatalysis, and numerous other reactions of industrial significance.[1] Much consideration must be made in selecting the optimal catalyst material for a given reaction: metals that cause too weak adsorption cannot effectively activate reactants, whereas metals that promote too strong adsorption cannot effectively desorb the products to allow for the binding of new reactant molecules. The result is a "volcano" shaped relationship between the catalytic rate and the binding energy (which will henceforth be called interchangeably as the adsorption energy).[2,3] This observation forms the basis of the Sabatier principle: the optimal choice corresponds to a surface with binding energies of moderate strength for the given adsorbates.[4,5] As such, binding energy is a key parameter in the selection of metal catalysts.

A class of linear relationships was proposed by Abild-Pedersen et al., who showed that the binding energies of CH_x, NH_x, OH_x, and SH_x species on various close-packed and stepped surfaces correlate linearly with the corresponding binding energies of C, N, O, and S atoms, respectively.[6] A similar analysis by Jones et al. demonstrated that several C_2 species on close-packed and stepped surfaces obey these linear trends well.[7] Kolb et al. focused on close-packed surfaces only and also observed linear scaling relationships between the binding energies of C and CH_x species.[8] Such scaling relations have been rationalized[6] using the d-band theory[9,10] through a

Received: January 30, 2025
Revised: May 30, 2025
Accepted: June 2, 2025
Published: June 11, 2025

separation of sp- and d-electron contributions to the binding energy. Specifically, the sp-electron contribution is expected to remain constant for a surface made of different transition metals, while the d-electron contribution is deemed the major factor underneath the scaling relations. Furthermore, the slope of these linear relations was attributed to the bond order conservation of the adsorbate atom,[6,11] whereby the additional "adsorbate-surface bonds" allow the adsorbate atom to achieve its maximum valency. Along this line, Kolb et al. studied the adsorption of COH and CH, both of which can form three bonds with the metal surface, versus C atom adsorption and found a similar slope for these two chemical species, further supporting the concept of bond order conservation.[8]

Several groups further generalized the linear scaling relations and d-band theory to more complex systems. Bhattacharjee et al. developed a spin-polarized d-band theory for 3d transition metal surfaces with unpaired electrons.[12] Ram et al. extended the scaling relations to magnetic bimetallic metal systems, where the slopes were found to depend not only on the adsorbates but also on the magnetic moment of the bimetallic surface.[13,14] Beyond the adsorption of a single adsorbate to a pristine metal surface, researchers also studied systems with adsorbate−adsorbate interactions or nonpristine surfaces. Miller et al. identified scaling relations for species adsorbed in different configurations, provided that the adsorption geometries are similar.[15] Later work by Majumdar and Greeley and by Brito-Ravicini and Calle-Vallejo showed that surface conditions can change the valency of the adsorbed atom either through adsorbate−adsorbate interactions[16] or adsorption to different slab facets,[17] leading to different slopes for the scaling relations across a series of metals.

In general, detailed quantum chemical analysis is needed to understand the origins of these intriguing scaling relations governing the binding energies.[6−17] (We note recent efforts toward understanding scaling relations for reaction energies.[18]) In addition to the d-band theory, bond order conservation of the adsorbate, and magnetic moment of metal surfaces, researchers also explored other factors such as electrostatics,[19] σ and π-bonding,[20] as well as strain due to adsorption and ligand effects on the adsorbate.[21] In the context of modern energy decomposition analysis,[22−26] which is routinely employed in atomic-orbital basis DFT calculations, the adsorbate can interact with the metal surface via four distinct mechanisms. First, the adsorbates can have strong electrostatic interactions with the metal surfaces, which may arise from the polarity of the adsorbate species and/or the overlap of the metal surface and adsorbate charge densities. Second, the adsorbates, especially highly polar ones, can also polarize the metal electron density. The reverse polarization can be equally important, where the metal surface perturbs the adsorbate orbitals and its electron density. Third, charge transfer is expected to make a substantial contribution to binding: many metal surfaces can readily donate electrons to the adsorbate, whereas back-donation from the adsorbate may also be significant, especially for surfaces of metal atoms with unfilled d orbitals. Lastly, van der Waals interactions are present to keep the adsorbate not too close to the metal surface (through short-range repulsion) and attract the adsorbates at a good distance away from the surface (through long-range dispersion). Thus, a unique perspective on the scaling relationship governing the binding energies can be obtained with all of these interaction energy components taken into account.

The present study aims to gain such a perspective on the causes of the linear scaling relations in the context of adsorption of CH_x species on fcc(100) transition metal surfaces. Specifically, plane-wave and atomic orbital DFT calculations and absolutely localized molecular orbital (ALMO) based energy decomposition analysis are performed to seek answers to two questions: *(1) Does each component (electrostatics, polarization, charge transfer, and van der Waals) of the binding energy follow a linear scaling relationship? (2) Can we further decompose these energy components into sp- and d-electron contributions and find the connection to the d-band model?*

2. METHODS

2.1. Absolutely Localized Molecular Orbitals Based Energy Decomposition Analysis (ALMO-EDA)

The binding energy of an adsorbate species A on a metal surface M to produce an adsorption complex AM can be calculated as

$$\Delta E_{ads} = E_{AM} - E_A - E_M \quad (1)$$

where E_{AM} is the energy of the adsorption complex, and E_A and E_M are the energies of the isolated adsorbate (A) and metal surface (M), respectively. For CH_x species (x = 1−4) on a specified surface, the linear scaling relationships are of the form

$$\Delta E_{ads}^{CH_x} = \alpha \Delta E_{ads}^{C} + \beta \quad (2)$$

It is common to focus on the lowest-energy binding configuration for each species on the surface, as will be done in the present work.

Below, the binding energies will be further decomposed into physically meaningful components using the energy decomposition analysis scheme based on Absolutely Localized Molecular Orbitals (ALMO-EDA).[26−30] Within the ALMO approach, the total binding energy is decomposed as

$$\Delta E_{ads} = \Delta E_{FRZ} + \Delta E_{POL} + \Delta E_{CT} \quad (3)$$

with terms for the frozen (FRZ), polarization (POL), and charge transfer (CT) interactions. The FRZ term corresponds to the energy change associated with bringing the infinitely separated fragments into their complex geometry, with no relaxation of the fragment molecular orbitals (MOs). The FRZ term can be further decomposed as

$$\Delta E_{FRZ} = \Delta E_{elec} + \Delta E_{Pauli} + \Delta E_{disp} \quad (4)$$

representing the (classical) electrostatic, Pauli repulsion, and dispersion interactions.[28,31] In this work, we combine the Pauli repulsion and dispersion terms into a single van der Waals (vdw) term

$$\Delta E_{vdw} = \Delta E_{Pauli} + \Delta E_{disp} \quad (5)$$

The POL term is the energy change associated with the relaxation of the MOs on each fragment in the presence of (the nuclei and electron density of) the other fragment, while keeping the MOs of each fragment "absolutely localized" (i.e., only expanded by the atomic orbital basis functions belonging to that fragment) such that CT between fragments is forbidden. The CT term is then defined as the energy change from the polarized state to the fully relaxed complex, where the MOs are permitted to delocalize between fragments.

Since it is possible for the spin state of the isolated adsorbate (i.e., in the FRZ stage) to differ from the spin state of the adsorbed species, an additional term corresponding to the spin flip (SF) energy will appear. It is defined as the difference between the fully relaxed DFT energies for the adsorbate−surface complex within two different spin states (e.g., triplet (T) and singlet (S))

$$\Delta E_{SF} = E_{FULL}^{(S)} - E_{FULL}^{(T)} \quad (6)$$

where "FULL" refers to the fully converged DFT solution for the adsorbate−metal cluster complex. When applicable, the SF contribution is included in the CT energy, as the most stable spin state usually changes upon charge transfer. A more detailed description of

https://doi.org/10.1021/jacsau.5c00111
JACS Au 2025, 5, 3092−3103

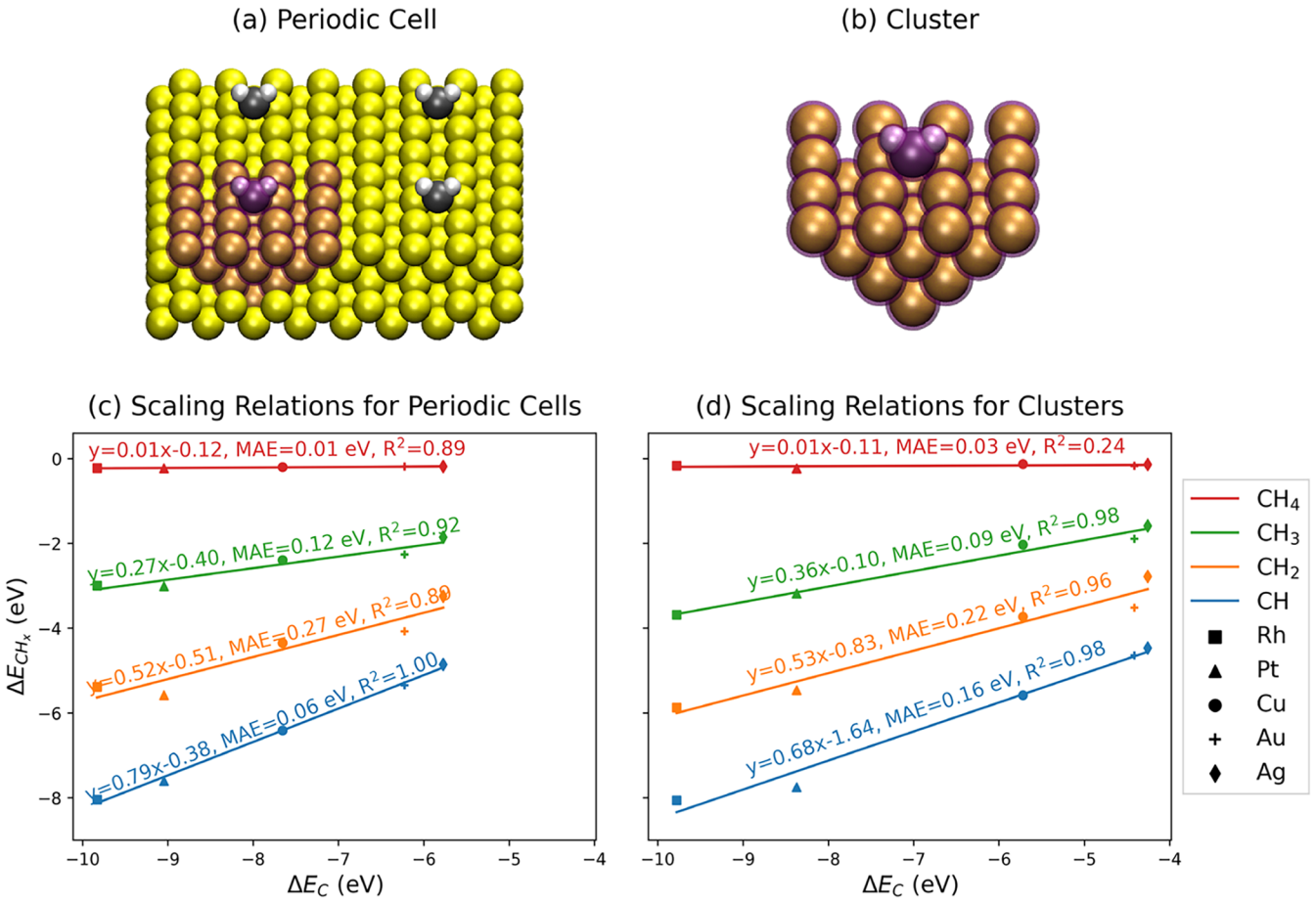

Figure 1. (a) An example adsorbate (CH_2) in the hollow site of a 4 × 4 × 4 unit cell of metal atoms. The metal atoms to be kept in the cluster model (b) are highlighted in brown. (b) A 30-atom metal cluster with CH_2 in the hollow site, as extracted from the periodic system (a). (c) Scaling relations for the CH_x species on 4 × 4 × 4 periodic cells based on adsorption energies (in eV) calculated using the PBE functional with VASP. (d) Scaling relations for the CH_x species on the 30-atom metal clusters, where the BSSE-corrected adsorption energies (in eV) are calculated using the PBE functional with Q-Chem. Both plots (c, d) show the binding energies for the lowest-energy sites.

the ALMO-EDA scheme can be found in the Supporting Information (Section S1).

2.2. Separation of sp and d Contributions to Polarization and Charge-Transfer Energies

The polarization and charge transfer energies, ΔE_{POL} and ΔE_{CT}, can be further decomposed into contributions from sp- and d-orbitals using a three-step procedure. In the first step, complementary occupied-virtual orbital pair (COVP) analysis is performed on both energy components.[32−34] In the second step, the weights of sp and d contributions are assessed for each occupied or virtual orbital assigned to the metal cluster. Specifically, for the qth fragment orbital with coefficients $\mathbf{C}_q$ (a single column vector), the corresponding "density matrix" can be written as

$$\tilde{\mathbf{P}}_q = \mathbf{C}_q \mathbf{C}_q^{\dagger} \tag{7}$$

which is normalized in the sense that

$$\sum_{\mu} (\mathbf{S}^{1/2} \tilde{\mathbf{P}}_q \mathbf{S}^{1/2})_{\mu\mu} = 1 \tag{8}$$

with $\mathbf{S}^{1/2}$ being the square root of the standard overlap matrix between atom-centered Gaussian basis functions, and μ indexing the basis functions. Then, the weight of the metal sp- or d-electron contributions can be computed by summing the diagonal elements of $\mathbf{S}^{1/2} \tilde{\mathbf{P}}_q \mathbf{S}^{1/2}$ associated with sp or d basis functions

$$w_{\mathrm{sp},q} = \sum_{\mu \in \mathrm{sp(M)}} (\mathbf{S}^{1/2} \tilde{\mathbf{P}}_q \mathbf{S}^{1/2})_{\mu\mu} \tag{9}$$

$$w_{\mathrm{d},q} = \sum_{\mu \in \mathrm{d(M)}} (\mathbf{S}^{1/2} \tilde{\mathbf{P}}_q \mathbf{S}^{1/2})_{\mu\mu} \tag{10}$$

The sum, $w_{sp} + w_d$, is close to 1.0 for both *occupied* and *virtual* COVP orbitals for *metal cluster polarization*, the *occupied* COVP orbitals for *metal-to-adsorbate charge transfer*, as well as the virtual orbitals for the *adsorbate-to-metal* charge transfer. It is slightly smaller than 1.0 because of the inclusion of f-basis functions on metal atoms (within the def2-SVP basis) and the use of projected virtual orbitals in the COVP charge transfer analysis.

In the third and final step, the polarization energy for a COVP-POL pair (i, a) on the metal cluster fragment is scaled by $w_{\mathrm{sp},i} w_{\mathrm{sp},a}$, $w_{\mathrm{sp},i} w_{\mathrm{d},a}$, $w_{\mathrm{d},i} w_{\mathrm{sp},a}$, and $w_{\mathrm{d},i} w_{\mathrm{d},a}$ to break it into sp → sp, sp → d, d → sp, and d → d contributions. Similarly, the COVP-CT energy for pair ($i \in$ metal, $a \in$ adsorbate) is scaled by $w_{\mathrm{sp},i}$ and $w_{\mathrm{d},i}$ to break the metal→ adsorbate charge transfer into sp and d contributions. Likewise, the COVP-CT energy for pair ($i \in$ adsorbate, $a \in$ metal) is scaled by $w_{\mathrm{sp},a}$ and $w_{\mathrm{d},a}$ to decompose the corresponding adsorbate → metal CT energy.

2.3. Metal−Adsorbate "Bond Order" Analysis

The bond order between the adsorbate and surface atoms represents the effective number of "bonds" formed between the two fragments. It can be calculated using the one-particle density matrices associated with the FRZ, POL, and FULL states, which are in turn computed from the occupied MO coefficients in each state. To ensure the

https://doi.org/10.1021/jacsau.5c00111
JACS Au 2025, 5, 3092−3103

idempotency of the FRZ and POL density matrices, one constructs the overlap matrix $\boldsymbol{\sigma}_{oo} = \mathbf{C}_{occ}^{\dagger}\mathbf{S}\mathbf{C}_{occ}$ among the occupied orbitals on both the metal and adsorbate fragments and uses it to construct the density matrix

$$\tilde{\mathbf{P}} = \mathbf{C}_{occ}(\boldsymbol{\sigma}_{oo}^{-1})\mathbf{C}_{occ}^{\dagger} \tag{11}$$

From this density matrix, we can compute the Löwdin occupancy for each basis function μ

$$n_{\mu} = (\mathbf{S}^{1/2}\tilde{\mathbf{P}}\mathbf{S}^{1/2})_{\mu\mu} \tag{12}$$

to assess the electronic configurations of the metal cluster and adsorbate. The off-diagonal block elements, $(\mathbf{S}^{1/2}\tilde{\mathbf{P}}\mathbf{S}^{1/2})_{\mu\nu}$ where $\mu \in$ metal (M) and $\nu \in$ adsorbate (A), can be employed to compute the "Mayer bond order"[35,36]

$$B_{ML} = 2\sum_{\mu\in M}\sum_{\nu\in A}(\mathbf{S}^{1/2}\tilde{\mathbf{P}}\mathbf{S}^{1/2})_{\mu\nu}(\mathbf{S}^{1/2}\tilde{\mathbf{P}}\mathbf{S}^{1/2})_{\nu\mu} \tag{13}$$

which captures the "bond order" (i.e., effective degree of electronic entanglement)[37] between the metal cluster and adsorbate. Note that eq 13 calculates the Mayer bond order of one spin. For closed-shell systems, its value needs to be further multiplied by 2, while for open-shell systems the α and β contributions need to be combined together.

3. COMPUTATIONAL DETAILS

The present study was conducted using 5 adsorbates (C atom and CH_x; $x = 1-4$) placed at 3 sites (ontop, bridge, hollow) on 5 different fcc(100) transition metal surfaces (Ag, Au, Cu, Pt, Rh), giving 75 distinct complexes. The lattice constants used for the respective metals were 4.09, 4.08, 3.61, 3.92, and 3.80 Å.[38] For each complex, 4 × 4 × 4 periodic cells were prepared using the Atomic Simulation Environment (ASE) package[39] as illustrated in Figure 1(a). The unit cells were separated by a vacuum of 20 Å in the z-direction, and the bottom two layers of each slab were held fixed.

All periodic calculations were performed using the VASP 5.4.1 package,[40−42] which uses a plane-wave basis and the projector augmented wave method and potpaw.52 pseudopotential.[43] An energy cutoff of 400 eV was used for the plane-wave basis, and a 4 × 4 × 1 Monkhorst−Pack k-point mesh was applied for Brillouin zone sampling.[44] Partial occupancies were determined using the first-order Methfessel-Paxton scheme[45] with a smearing width of k_BT = 0.2 eV, while the final energies were extrapolated back to an electronic temperature of k_BT = 0.0 eV. The blocked-Davidson[41,42] and RMM-DIIS[41,42,46] algorithms were used for the electronic minimization, and a conjugate gradient algorithm[47] was used for the geometry relaxation. Energy convergence criteria of 10^{-6} and 10^{-4} eV were used for the electronic and ionic updates, respectively. The dipole correction was not used when calculating the adsorption energies.

Next, clusters of 30 metal atoms were cut from the relaxed periodic slabs in an "inverted pyramid" configuration, as shown in Figure 1(a,b). This was inspired by the use of inverted pyramids in the modeling of other adsorbate−surface systems.[48] All cluster calculations were performed using the Q-Chem 6.2 package.[49] The def2-SVP[50,51] basis set was used for all cluster calculations. All-electron calculations were performed for Cu, whereas the ECPs associated with the Karlsruhe "def2" basis sets[51] were used to represent the core electrons of the heavier atoms (Ag, Au, Pt, Rh). Counterpoise-corrected[52] calculations were performed to assess the effects of basis set superposition error (BSSE) on the binding energies. BSSE-uncorrected calculations were performed using the ALMO-EDA[26−30] scheme to decompose the interaction energies. The fragment spin alignment procedure introduced in ref 30 was disabled to aid with convergence. The classical decomposition of the frozen interaction[53] with the modified Pauli repulsion term[31] was used due to the use of ECPs, which restricts the availability of the orthogonal decomposition scheme[28] for metals heavier than Cu. The fragment-wise polarization and fragment-pairwise charge-transfer terms were calculated using the nonperturbative (variational) approaches,[33,34] and the orbital-based analyses of these terms were performed using complementary occupied-virtual pairs (COVPs) with a COVP threshold of 0.5 kJ/mol. ALMO-EDA calculations for C and CH_2 in both the singlet and triplet spin states were performed to obtain the spin flip contributions. The geometric direct minimization (GDM)[54] algorithm was used for the energy minimization of the electronic states involved in ALMO-EDA calculations, with a convergence criterion of 10^{-6} a.u. for the root-mean-square of the orbital rotation gradient. To check the effect of the cluster size, we also embedded the carbon atom in the hollow site of a larger Cu_{54} cluster. The total binding energy and ALMO energy components are shown in Supporting Information Table S10 to change only slightly with the increase in the cluster size.

All calculations were performed using the Perdew−Burke−Ernzerhof (PBE) functional[55] and the DFT-D3(BJ) dispersion correction.[56,57] As a comparison, the case of a carbon atom adsorbed onto the hollow site of a Cu surface was also subjected to periodic and cluster calculations with the RPBE functional,[58] which has been widely used in DFT modeling of metal surface catalysis. As shown in SI Table S11, the adsorption energies (and the ALMO energy components obtained from the cluster calculations) are only marginally different with the PBE and RPBE functionals. Additional cluster calculations were performed using a hybrid functional, PBE0,[59] and a range-separated hybrid functional, HSE-HJS.[60,61] Total adsorption energy (Figures S3 and S4) and ALMO energy components (Figures S5 and S6) show linear scaling relations for the PBE0 and HSE-HJS functionals. However, the slopes exhibit larger deviations from the ideal scaling slopes than PBE.

4. RESULTS

4.1. Scaling Relationships of Total Adsorption Energies

The scaling relationships in the total binding energies for CH_x ($x = 1-4$) species relative to the C atom on the 5 metal surfaces in the lowest energy sites are presented for the periodic calculations in Figure 1(c) and for the cluster calculations in Figure 1(d). For both the periodic and the cluster models, it can be observed in Tables S1−S5 that C and CH prefer the hollow site; CH_2 favors the bridge site in most cases and the hollow site in other cases; CH_3 prefers the bridge and ontop sites equally; CH_4 does not show any site preference. These results on preferred binding sites agree with previous reports.[6,8]

For the periodic systems, the scaling relationships from our calculations also agree with previous works. In Figure 1(c), the fitted slopes (0.79, 0.52, 0.27, and 0.01) closely follow the previously suggested adsorbate valency based values of $(4 - x)/4$ for CH_x.[6,8] The deviation from perfectly linear scaling relations is rather minor, with the largest mean absolute error (MAE) being 0.27 eV for the adsorption energies (which range over several eVs) and the R^2 values all exceeding 0.80.

https://doi.org/10.1021/jacsau.5c00111
JACS Au 2025, 5, 3092−3103

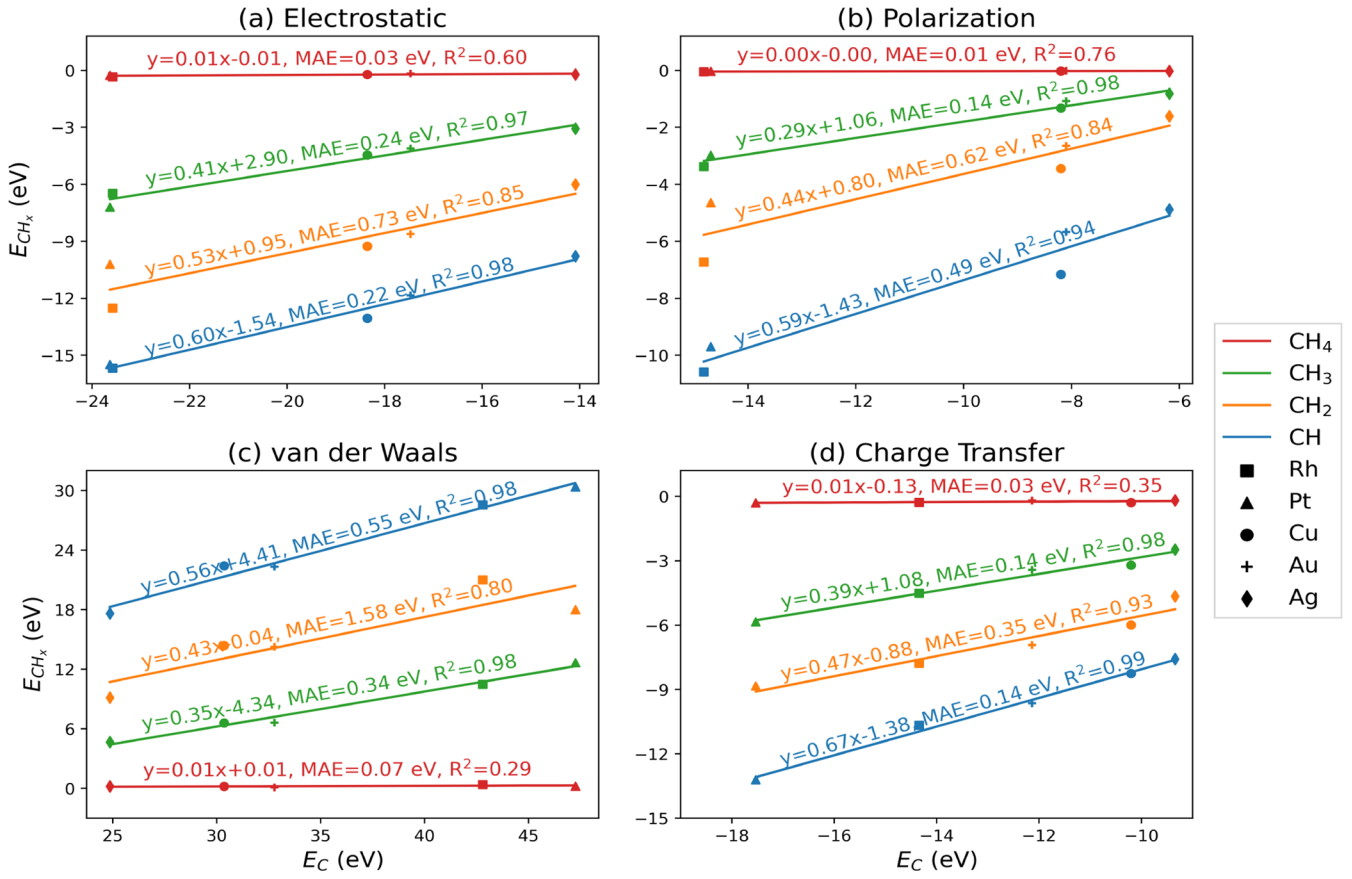

Figure 2. Scaling relations of ALMO-EDA energy components for the CH_x species on the 30-atom metal (Cu, Au, Ag, Rh, Pt) clusters: (a) electrostatic, (b) polarization, (c) van der Waals, and (d) charge transfer. The energy components were calculated using Q-Chem for the lowest-energy spin states at the lowest-energy binding sites.

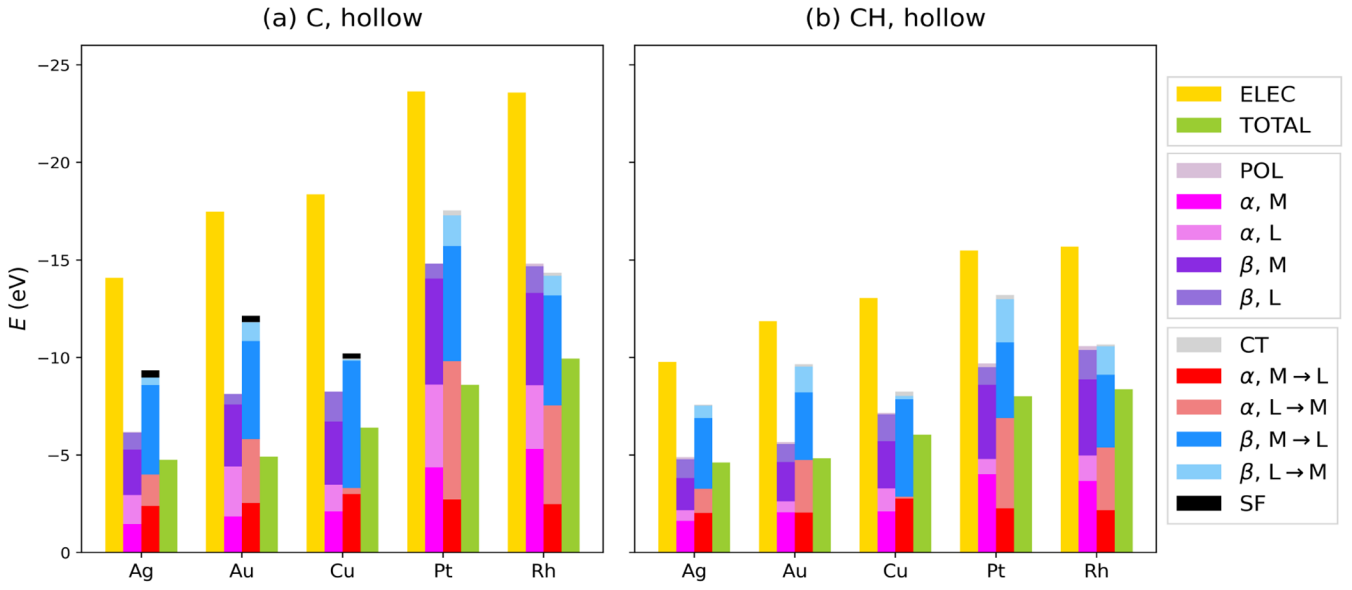

Figure 3. Attractive ALMO-EDA energy components (in eV) for (a) C and (b) CH in the hollow site of 30-atom metal clusters. The main COVP contributions (>5.2 meV) from α and β electrons of the metal (M) and the adsorbate (L) to the polarization and charge transfer energies are highlighted, with the remaining smaller contributions being shown in thistle (POL) and gray (CT). The spin flip energy (SF; triplet → singlet, for the applicable systems) is shown in black and included in the charge transfer energy. Similar plots for other species/sites may be found in the Supporting Information.

For the cluster models, the adsorption energies show a good correlation (R^2 = 0.93) with the value for the corresponding periodic systems (Figure S1). The small deviations in the adsorption energies can be ascribed to the different basis functions in use (plane wave vs atom-centered Gaussian functions) and the truncated sizes for the clusters. After all, the

https://doi.org/10.1021/jacsau.5c00111
JACS Au 2025, 5, 3092−3103

adsorption energies of adsorbates on transition metal clusters can exhibit some oscillation as the size of the cluster grows toward a full, infinite surface.[62] Despite the differences, the general trends of the scaling relations for the periodic systems are reproduced well by the cluster model resulting in Figure 1(d), with the fitted slopes being 0.68, 0.53, 0.36, and 0.01, respectively, for the CH_x adsorbates, an MAE up to 0.22 eV from the linear fitting values, and an R^2 value of 0.96 or higher for CH_x (x = 1, 2, 3). This establishes the validity of using the truncated metal clusters as surrogate models for the periodic surfaces for carrying out further energy decomposition analysis.

4.2. Scaling Relationship of Adsorption Energy Components

To explore the scaling relations for individual energy components, all values are computed within the ALMO-EDA framework and tabulated in Tables S1−S5. As shown in Figure 2, for all adsorbates (C, CH, CH_2, CH_3, and CH_4) on the five metal surfaces, the electrostatic, polarization, and charge transfer interactions stabilize the respective complexes, whereas the van der Waals interactions are dominated by Pauli repulsion and thus weaken the binding.

The attractive ALMO-EDA energy components are shown in detail in Figure 3 for two representative cases, C and CH at the hollow site of the various metals. Here the electrostatic interaction is shown to contribute the most to the total adsorption energy. As shown in Tables S1−S5, this is generally true for the hollow and bridge sites but not for the ontop site, where the charge-transfer contribution dominates. The strikingly large electrostatic interactions in these systems arise from the close contact between the adsorbates (save CH_4) and the metal surface (Table S9), in particular for species adsorbed at the hollow site. At such short distances, the charge distribution of the interacting species overlap, leading to extraordinarily large electrostatic interactions also known as the charge penetration effect.[31,63] The charge penetration contribution decays exponentially with the intermolecular separation, which accounts for the diminished role of electrostatics for the ontop adsorptions. While the electrostatic component makes the greatest contribution among the attractive terms and exhibits the same trend as the total binding energy across these systems, i.e., both ΔE_{ELEC} and ΔE_{FULL} are more favorable with Pt and Rh, we note that this attractive contribution is offset entirely by Pauli repulsion (Figure S2), which is typical for intermolecular complexes where the electron densities of the two monomers strongly overlap with each other.[28,64] As shown in Figure S2, the trend is reversed when electrostatics is combined with Pauli repulsion, with Rh and Pt having less favorable "E + P" contributions. Therefore, the frozen interaction in these systems makes a net positive contribution and thus does *not* provide the driving force for the adsorption. *The polarization and charge transfer interactions are essential to achieve an overall favorable binding.*

In terms of the scaling relationships, Figure 2 shows that *all four energy components (electrostatic, polarization, van der Waals, and charge transfer) for* CH_x *(x = 1, 2, 3) adsorption exhibit remarkable linear correlations with the corresponding values for the adsorbed carbon atom.* The R^2 values are all above 0.80, which are comparable to the R^2 values for the total adsorption energies in Figure 1. Among all energy components, the linear scaling relations in Figure 2(d) for the charge transfer energies are especially robust, with R^2 reaching 0.93−0.99.

It should be noted that compared to the total adsorption energy, all of the energy components display a larger MAE from the linearly fitted values. This is particularly noticeable for CH_2, for which the MAEs for energy components fall in the range of 0.35 eV (charge transfer) to 1.58 eV (van der Waals). To a large extent, this is caused by the larger magnitudes of individual energy components than that of the total adsorption energy. For instance, the van der Waals contribution (as dominated by Pauli repulsion) is as large as 21.004 eV (the orange square in Figure 2(c)) for the CH_2−Rh_{30} complex, whereas the total adsorption energy (without BSSE correction) is only −6.021 eV.

In terms of the slopes, all individual components also follow the general trend observed for the total scaling relations in that the slope becomes smaller with decreasing valency of the adsorbate (i.e., from CH to CH_4). But the slopes from the energy component scaling relations differ more substantially from the suggested theoretical values—0.75 (CH), 0.50 (CH_2), and 0.25 (CH_3)—than those observed in Figure 1 for the total adsorption energies. Here in Figure 2, the slopes of charge transfer energies (0.67/0.47/0.39) and polarization energies (0.59/0.44/0.29) deviate less substantially from above theoretical values than the slopes of electrostatic (0.60/0.53/0.41) and van der Waals (0.56/0.43/0.35) energies, suggesting the potentially more substantial roles of POL and CT in leading to the slopes of the total adsorption energies.

4.3. COVP Analysis of Polarization and Charge Transfer Energies

As mentioned above, the polarization and charge transfer energies are key driving forces of the adsorbate-metal binding. To further understand these interactions, the ALMO-based COVP analysis is employed to elucidate their physical origins by further breaking them into fragment-wise or fragment-pairwise contributions.

The polarization can arise from the occupied-virtual orbital mixing within the adsorbate (as polarized by metal surface) or those within the metal cluster (in response to the nuclei and electron densities of the adsorbate). As shown in Figure 3(a), when located in the hollow site of metal surfaces, a C atom (L, the ligand) is mainly perturbed through its α electrons. Specifically, as shown in Figure 4(a), the $2p_x$ orbital of a C atom on Pt surface loses 0.905 α electrons to its $2p_z$ orbital. Note that the amount of migrated charge (ΔQ) here is calculated based on the analysis scheme associated with the COVPs;[33,34] using basis function occupancy based on Löwdin population, this value is estimated to be 0.540 e^- (Table S8). Meanwhile, the polarization energy within the Pt and Rh metal clusters, which is nearly equally distributed among the α and β electrons, is higher than those for Ag/Au/Cu clusters. This is expected because the Pt and Rh clusters, with an average d^9s^1 and d^8s^1 electronic configuration for each metal atom (see Table S7), respectively, have empty d orbitals to accept electrons (see Figure 4(b) for the case of C−Pt_{30}), in contrast to the $d^{10}s^1$ Ag/Au/Cu atoms. For a CH molecule on the metal surface, Figure 3(a) shows much smaller polarization energy for the adsorbate, and slightly weaker polarization of the metal surface.

When it comes to charge transfer, the strength of α and β M → L charge transfer to C and CH_2 adsorbates are approximately constant across the metals in Figure 3. As an example, Figure 4(d) shows that 0.178 α electrons (0.131 e^- in Table S8) migrated from mostly the d orbitals of the 4 closest

https://doi.org/10.1021/jacsau.5c00111
JACS Au 2025, 5, 3092−3103

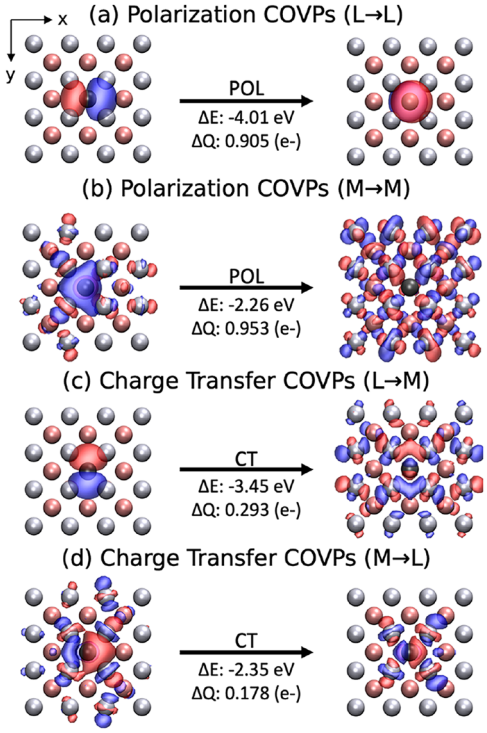

Figure 4. Representative COVP orbitals for carbon adsorbed on the Pt surface at the *hollow* site. (a–d) α-COVP donor–acceptor pairs for (a) L → L polarization, (b) M → M polarization, (c) L → M charge transfer, and (d) M → L charge transfer. Pt atoms below the first layer are pink, first-layer Pt atoms are silver, and carbon atoms are gray. ΔE is the energy lowering due to the transfer of ΔQ electrons from the donor orbital of one fragment to the acceptor orbital on the same (for POL) or another (for CT) fragment.

Pt atoms to the $2p_x$ orbital of the C atom (whose occupancy was reduced during the polarization stage). On the other hand, the L → M donation was more substantial in the cases of Pt_{30} and Rh_{30}, where electrons can be injected into the partially filled d orbitals of the clusters. For instance, 0.293 e^- (0.418 e^- in Table S8) was transferred from the $2p_y$ orbital of C atom to the d orbitals of the neighboring and farther-away Pt atoms shown in Figure 4(c).

In terms of the relative α vs β contributions to these charge transfer energies, L → M donation mostly involves α electrons. This is expected because C and CH adsorbates have more α electrons than β ones. Conversely, M → L CT is dominated by the donation of metal β electrons to the empty β orbitals of the adsorbate.

4.4. Separation of sp and d Contributions to the Polarization and Charge Transfer Energies

As mentioned in the introduction, the scaling relationship was rationalized by Nørskov and co-workers[6] with the d-band theory[9,10] that states the differences in adsorption energies across the metals is mostly due to interactions with the d states. As such, it invoked a separation of contributions to adsorption energy from sp and d electrons of transition metals. The sp-electron contribution was suggested to remain nearly constant from metal to metal, whereas the d-electron contribution varies more substantially and underlies the observed linear scaling relationship. To explore this in the context of adsorption on the cluster model of metal surfaces, a further separation of the polarization and charge transfer energies into their sp and d orbital contributions is carried out using the procedure described in Section 2.2, producing the results shown in Figure 5.

In panel (a) of Figure 5, the sp → sp polarization energies are clearly similar across the metals Ag, Au, and Cu; but they are significantly lower for Pt and Rh, as it becomes easier to polarize sp electrons into the empty d orbitals of these metal atoms instead, resulting in their more pronounced sp → d polarization. The α and β d → sp contributions to the polarization energy do not differ much among the metals, which is expected as each metal has a $d^n s^1$ electron configuration on average. The most striking differences in polarization reside in the d → d contributions, which are much larger for Pt and Rh (again due to their empty d orbitals) than for the other metals. This confirms that the variation in the polarization energy of the $C–M_{30}$ complexes arise primarily from d electrons of the metal atoms.

Similar conclusions may be drawn on the charge transfer interaction shown in Figure 5(b). The net metal sp-electron contributions to charge transfer energy (M-sp → L and L → M-sp, see first column for each metal) appear to be rather

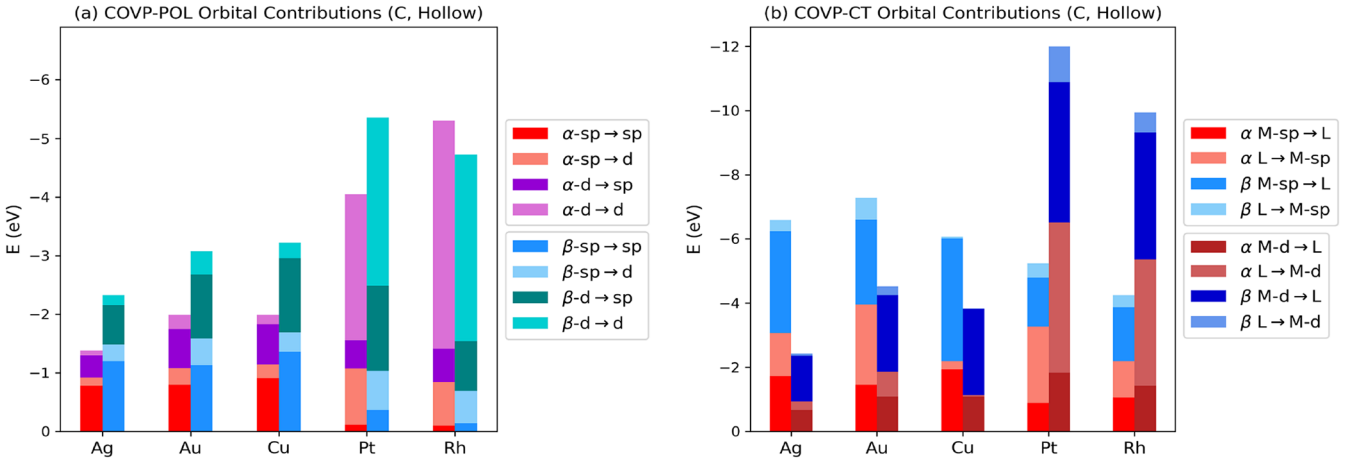

Figure 5. (a) COVP-POL energy contributions from transition metal's sp and d orbitals for M → M polarization. (b) COVP-CT energy contributions from the sp and d orbitals of the metal atoms for M → L and L → M CT. All decompositions were performed using the triplet electronic configuration.

https://doi.org/10.1021/jacsau.5c00111
JACS Au 2025, 5, 3092–3103

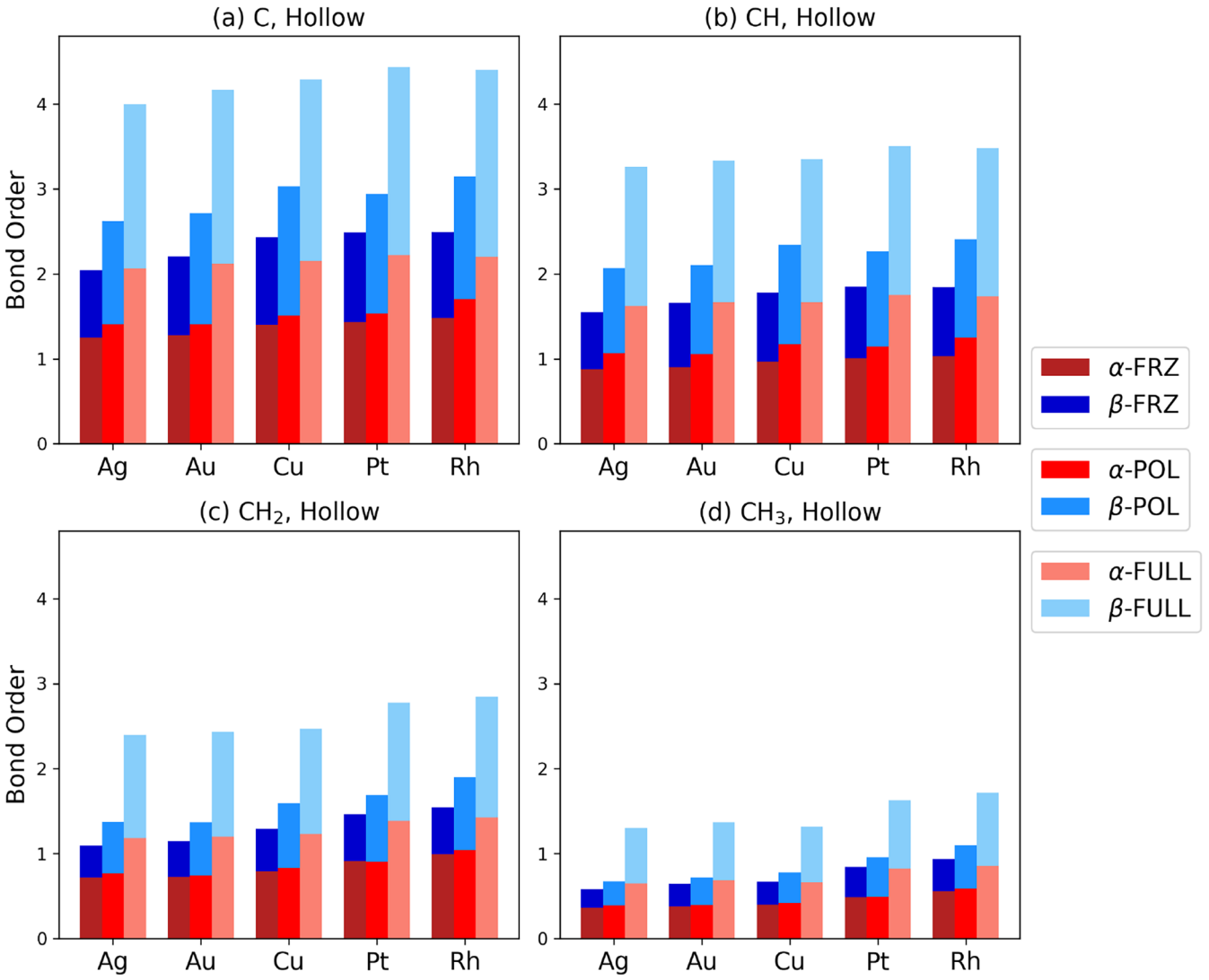

Figure 6. Calculated "Mayer bond orders" for the frozen (FRZ), polarized (POL), and fully converged SCF (FULL) states for the adsorption of (a) C, (b) CH, (c) CH_2, and (d) CH_3 onto the hollow site of each metal cluster.

consistent for Ag, Au, and Cu and actually decrease slightly for Pt and Rh. In contrast, the net metal d-electron contribution to the charge transfer (second column for each metal, mainly through α L → M-d and β M-d → L donations) is much greater for Pt and Rh.

Together, these findings within ao-KSDFT offer further support to the d-band model: *the variation in the adsorption energies of* CH_x *on the metal surfaces, especially the polarization and charge transfer components, arise mainly from contributions from metal d-electrons.*

4.5. Effective "Bond Order" between Adsorbates and Metal Clusters

As seen earlier in Figure 1, CH_x binds progressively weaker to the five metal surfaces as the number of hydrogen atoms in the adsorbate increases. This is expected on the ground of lowering valency of the adsorbates. In this work, a new metric—effective Mayer "bond order" between the adsorbate and metal surface—is computed according to eq 13 and shown in Figure 6 for the cases of hollow-site adsorption.

For the FULL state of all complexes, the metal−adsorbate "bond orders" are predicted to be slightly over 4 (C), 3 (CH), 2 (CH_2), and 1 (CH_3), which are in remarkable agreement with the valency of these adsorbates. As far as other ALMO-EDA states are concerned, the "bond orders" acquire only half of their values at the FRZ stage and increase slightly with the incorporation of mutual polarization. Charge transfer, therefore, is key for each adsorbate to fully reach its maximum valency. This reaffirms the bond order conservation underlying the observed scaling relations.[11]

5. DISCUSSION

This work has focused on an ALMO-based analysis of the interaction between a CH_x adsorbate and a metal cluster. Clearly, it would be desirable to connect and compare the ALMO results to those from the popular Newns-Anderson model.[65−71] Here, we briefly demonstrate how an Anderson Hamiltonian can be built for the systems under consideration.

Starting from the noninteracting metal surface and adsorbate fragment orbitals, $\mathbf{C}_{\mathrm{M}}^{(0)}$ and $\mathbf{C}_{\mathrm{A}}^{(0)}$, one can use the standard AO basis overlap matrix, $\mathbf{S}$, to obtain the overlap between the fragment orbitals

https://doi.org/10.1021/jacsau.5c00111
JACS Au 2025, 5, 3092−3103

$$\mathbf{S}_{\mathrm{FRZ}} = \begin{bmatrix} \mathbf{I}_{\mathrm{M}} & \mathbf{C}_{\mathrm{M}}^{(0),\dagger}\mathbf{S}\mathbf{C}_{\mathrm{A}}^{(0)} \\ \mathbf{C}_{\mathrm{A}}^{(0),\dagger}\mathbf{S}\mathbf{C}_{\mathrm{M}}^{(0)} & \mathbf{I}_{\mathrm{A}} \end{bmatrix}$$

The corresponding (idempotent) density matrix in the AO basis is

$$\mathbf{P}^{(0)} = [\mathbf{C}_{\mathrm{occ,M}}^{(0)} \quad \mathbf{C}_{\mathrm{occ,A}}^{(0)}]\mathbf{S}_{\mathrm{occ,FRZ}}^{-1}\begin{bmatrix} \mathbf{C}_{\mathrm{occ,M}}^{(0),\dagger} \\ \mathbf{C}_{\mathrm{occ,A}}^{(0),\dagger} \end{bmatrix}$$

where $\mathbf{C}_{\mathrm{occ,M}}^{(0)}$ and $\mathbf{C}_{\mathrm{occ,A}}^{(0)}$ refer to the occupied fragment orbitals, and $\mathbf{S}_{\mathrm{occ,FRZ}}$ the occupied-occupied sublock of $\mathbf{S}_{\mathrm{FRZ}}$. The corresponding atomic-basis Fock matrix, $\mathbf{F}^{(0)}$, can be built and then recast in the basis of fragment orbitals

$$\mathbf{F}_{\mathrm{FRZ}} = \begin{bmatrix} \mathbf{C}_{\mathrm{M}}^{(0),\dagger}\mathbf{F}^{(0)}\mathbf{C}_{\mathrm{M}}^{(0)} & \mathbf{C}_{\mathrm{M}}^{(0),\dagger}\mathbf{F}^{(0)}\mathbf{C}_{\mathrm{A}}^{(0)} \\ \mathbf{C}_{\mathrm{A}}^{(0),\dagger}\mathbf{F}^{(0)}\mathbf{C}_{\mathrm{M}}^{(0)} & \mathbf{C}_{\mathrm{A}}^{(0),\dagger}\mathbf{F}^{(0)}\mathbf{C}_{\mathrm{A}}^{(0)} \end{bmatrix} \tag{14}$$

which *corresponds to the Anderson Hamiltonian*. Through solving the generalized eigenvalue problem

$$\mathbf{F}_{\mathrm{FRZ}}\mathbf{C}' = \mathbf{S}_{\mathrm{FRZ}}\mathbf{C}'\lambda \tag{15}$$

one can obtain a new density matrix

$$\mathbf{P}' = \mathbf{C}'_{\mathrm{occ}}(\mathbf{C}'_{\mathrm{occ}})^{\dagger} \tag{16}$$

and estimate the energy change

$$\Delta E = \mathbf{F}_{\mathrm{FRZ}}\cdot(\mathbf{P}' - \mathbf{P}^{(0)}) \tag{17}$$

which corresponds to the polarization and charge transfer portions of the adsorption energy. Numerical analysis is underway to compare these results with those of the Newns-Anderson model, which will be reported in a forthcoming paper.

6. CONCLUSIONS

In this work, the binding energy between CH_x adsorbates and five fcc(100) transition metal surfaces have been decomposed using the ALMO-EDA scheme to gain more in-depth insights into the linear scaling relations between the adsorption energies of CH_x species and that of a C atom. Our main findings are as follows.

- For CH_x molecules, their adsorption to the metal surface can be described using truncated 30-atom clusters (M_{30}) as surrogate models, which yield good correlation with periodic DFT results (R^2 = 0.93).
- Polarization and charge transfer interactions between the adsorbates and the metal cluster are essential to achieve an overall favorable binding.
- The ALMO-EDA components (electrostatic, van der Waals, polarization, and charge transfer) all exhibit their own scaling relations, which follow the general trends observed in those for the total binding energy.
- The further decomposition of polarization and charge-transfer based on COVPs and the quantification of metal's sp- and d-electron contributions show that the variations in these terms on different metal surfaces primarily arise from the varying character of the d orbitals of each metal, which is fully consistent with the d-band theory.

As such, ALMO-EDA stands as a powerful tool for a detailed analysis of the interactions between adsorbates and metal surfaces. In addition, basis function occupancies and adsorbate-metal "bond orders" are also useful, intuitive metrics for characterizing the electronic structure of adsorbate-metal complexes. Equipped with these tools, one can investigate a broader range of surface−adsorbate interactions, including systems with more complex chemical compositions of the surface or the adsorbate. From a computational methodology standpoint, an extension of these analysis tools to periodic DFT calculations would be highly desirable. It will also be interesting to explore the effects of solvents[72] or microcavity[73] on the adsorption energies, which will require a further development of our EDA framework.

■ ASSOCIATED CONTENT

Supporting Information

The Supporting Information is available free of charge at https://pubs.acs.org/doi/10.1021/jacsau.5c00111.

Description of the ALMO-EDA procedure, periodic and cluster calculation results, additional calculations and benchmarks (PDF)

Adsorbate-metal surface geometries POSCAR (ZIP)

Adsorbate-metal surface geometries CLUSTER XYZ (ZIP)

■ AUTHOR INFORMATION

Corresponding Authors

Yuezhi Mao − *Department of Chemistry and Biochemistry, San Diego State University, San Diego, California 92182, United States;* orcid.org/0000-0001-5362-4333; Email: ymao2@sdsu.edu

Yihan Shao − *Department of Chemistry and Biochemistry, University of Oklahoma, Norman, Oklahoma 73019, United States;* orcid.org/0000-0001-9337-341X; Email: yihan.shao@ou.edu

Authors

Jesse DiCenso − *School of Sustainable Chemical, Biological, and Materials Engineering, Gallogly College of Engineering, University of Oklahoma, Norman, Oklahoma 73019, United States*

Chance Lander − *Department of Chemistry and Biochemistry, University of Oklahoma, Norman, Oklahoma 73019, United States*

Zheng Pei − *Department of Chemistry and Biochemistry, University of Oklahoma, Norman, Oklahoma 73019, United States;* orcid.org/0000-0002-1230-4664

Sanghita Sengupta − *Department of Chemistry and Biochemistry, University of Oklahoma, Norman, Oklahoma 73019, United States*

Tien Le − *School of Sustainable Chemical, Biological, and Materials Engineering, Gallogly College of Engineering, University of Oklahoma, Norman, Oklahoma 73019, United States;* orcid.org/0000-0003-2879-0828

Yu Zhang − *Theoretical Division, Los Alamos National Laboratory, Los Alamos, New Mexico 87545, United States;* orcid.org/0000-0001-8938-1927

G. T. Kasun Kalhara Gunasooriya − *School of Sustainable Chemical, Biological, and Materials Engineering, Gallogly College of Engineering, University of Oklahoma, Norman,*

https://doi.org/10.1021/jacsau.5c00111
JACS Au 2025, 5, 3092−3103

Oklahoma 73019, United States; orcid.org/0000-0003-1258-7841

Bin Wang − *School of Sustainable Chemical, Biological, and Materials Engineering, Gallogly College of Engineering, University of Oklahoma, Norman, Oklahoma 73019, United States;* orcid.org/0000-0001-8246-1422

Complete contact information is available at: https://pubs.acs.org/10.1021/jacsau.5c00111

Author Contributions

⊥J.D.C. and C.L. contributed equally to this work.

Notes

The authors declare no competing financial interest.

■ ACKNOWLEDGMENTS

Y.S. acknowledges the National Science Foundation grant CHE-2102071 for supporting part of this study, specifically the spin-crossing adsorption of C and CH_2 on metal surfaces. C.L and Y.Z. thank the support from the US DOE, Office of Science, Basic Energy Sciences, Chemical Sciences, Geosciences, and Biosciences Division under Triad National Security, LLC ("Triad") contract Grant 89233218CNA000001 (FWP: LANLECF7). Los Alamos National Laboratory is operated by Triad National Security, LLC, for the National Nuclear Security Administration of the US Department of Energy (Contract No. 89233218CNA000001) YM acknowledges the support from San Diego State University Startup Fund and SDSU Seed Grant. Y.S. thanks the O.U. Supercomputing Center for Education & Research (OSCER) for the computational resources. Financial support was provided by the University of Oklahoma Libraries' Open Access Fund.

■ REFERENCES

(1) Liu, L.; Corma, A. Metal Catalysts for Heterogeneous Catalysis: From Single Atoms to Nanoclusters and Nanoparticles. *Chem. Rev.* **2018**, *118*, 4981−5079.
(2) Hammer, B.; Nørskov, J. Theoretical Surface Science and Catalysis—Calculations and Concepts. *Adv. Catal.* **2000**, *45*, 71−129.
(3) Medford, A. J.; Moses, P. G.; Jacobsen, K. W.; Peterson, A. A. A Career in Catalysis: Jens Kehlet Nørskov. *ACS Catal.* **2022**, *12*, 9679−9689.
(4) Sabatier, P. *La Catalyse en Chimie Organique*; C. Béranger, 1920.
(5) Medford, A. J.; Vojvodic, A.; Hummelshøj, J. S.; Voss, J.; Abild-Pedersen, F.; Studt, F.; Bligaard, T.; Nilsson, A.; Nørskov, J. K. From the Sabatier Principle to a Predictive Theory of Transition-Metal Heterogeneous Catalysis. *J. Catal.* **2015**, *328*, 36−42.
(6) Abild-Pedersen, F.; Greeley, J.; Studt, F.; Rossmeisl, J.; Munter, T. R.; Moses, P. G.; Skúlason, E.; Bligaard, T.; Nørskov, J. K. Scaling Properties of Adsorption Energies for Hydrogen-Containing Molecules on Transition-Metal Surfaces. *Phys. Rev. Lett.* **2007**, *99*, No. 016105.
(7) Jones, G.; Studt, F.; Abild-Pedersen, F.; Nørskov, J. K.; Bligaard, T. Scaling Relationships for Adsorption Energies of C2 Hydrocarbons on Transition Metal Surfaces. *Chem. Eng. Sci.* **2011**, *66*, 6318−6323.
(8) Kolb, M. J.; Loffreda, D.; Sautet, P.; Calle-Vallejo, F. Structure-Sensitive Scaling Relations Among Carbon-Containing Species and their Possible Impact on CO2 Electroreduction. *J. Catal.* **2021**, *395*, 136−142.
(9) Hammer, B.; Nørskov, J. Electronic Factors Determining the Reactivity of Metal Surfaces. *Surf. Sci.* **1995**, *343*, 211−220.
(10) Hammer, B.; Norskov, J. K. Why Gold is the Noblest of All the Metals. *Nature* **1995**, *376*, 238−240.
(11) Shustorovich, E. Activation barrier for adsorbate surface diffusion, heat of chemisorption, and adsorbate registry: theoretical interrelations. *J. Am. Chem. Soc.* **1984**, *106*, 6479−6481.
(12) Bhattacharjee, S.; Waghmare, U. V.; Lee, S.-C. An improved d-band model of the catalytic activity of magnetic transition metal surfaces. *Sci. Rep* **2016**, *6*, No. 35916.
(13) Ram, S.; Lee, S.-C.; Bhattacharjee, S. Adsorption energy scaling relation on bimetallic magnetic surfaces: role of surface magnetic moments. *Phys. Chem. Chem. Phys.* **2020**, *22*, 17960−17968.
(14) Ram, S.; Lee, S.-C.; Bhattacharjee, S. Identifying the Critical Surface Descriptors for the Negative Slopes in the Adsorption Energy Scaling Relationships via Density Functional Theory and Compressed Sensing. *J. Phys. Chem. Lett.* **2021**, *12*, 9791−9799.
(15) Miller, S. D.; İnoğlu, N.; Kitchin, J. R. Configurational correlations in the coverage dependent adsorption energies of oxygen atoms on late transition metal fcc(111) surfaces. *J. Chem. Phys.* **2011**, *134*, No. 104709.
(16) Majumdar, P.; Greeley, J. Generalized scaling relationships on transition metals: Influence of adsorbate-coadsorbate interactions. *Phys. Rev. Mater.* **2018**, *2*, No. 045801.
(17) Brito-Ravicini, A.; Calle-Vallejo, F. Interplaying coordination and ligand effects to break or make adsorption-energy scaling relations. *Exploration* **2022**, *2*, No. 20210062.
(18) Kron, K. J.; Sharada, S. S. Linear Scaling Relationships in Homogeneous Photoredox Catalysis. React. *Chem. Eng.* **2024**, *9*, 3105−3109.
(19) Choksi, T.; Majumdar, P.; Greeley, J. P. Electrostatic Origins of Linear Scaling Relationships at Bifunctional Metal/Oxide Interfaces: A Case Study of Au Nanoparticles on Doped MgO Substrates. *Angew. Chem. Int. Ed* **2018**, *57*, 15410−15414.
(20) Vogt, C. Adsorbate Bond Number Dependency for σ- and π-bonds in Linear Scaling Relationships. *J. Phys. Chem. C* **2023**, *127*, 5416−5424.
(21) Mehta, P.; Greeley, J.; Delgass, W. N.; Schneider, W. F. Adsorption Energy Correlations at the Metal−Support Boundary. *ACS Catal.* **2017**, *7*, 4707−4715.
(22) Phipps, M. J. S.; Fox, T.; Tautermann, C. S.; Skylaris, C.-K. Energy decomposition analysis approaches and their evaluation on prototypical protein−drug interaction patterns. *Chem. Soc. Rev.* **2015**, *44*, 3177−3211.
(23) Zhao, L.; von Hopffgarten, M.; Andrada, D. M.; Frenking, G. Energy decomposition analysis. *WIREs: Comput. Mol. Sci.* **2018**, *8*, No. e1345.
(24) Mo, Y.; Bao, P.; Gao, J. Energy decomposition analysis based on a block-localized wavefunction and multistate density functional theory. *Phys. Chem. Chem. Phys.* **2011**, *13*, 6760−6775.
(25) Su, P.; Tang, Z.; Wu, W. Generalized Kohn-Sham energy decomposition analysis and its applications. *WIREs: Comput. Mol. Sci.* **2020**, *10*, No. e1460.
(26) Mao, Y.; Loipersberger, M.; Horn, P. R.; Das, A.; Demerdash, O.; Levine, D. S.; Prasad Veccham, S.; Head-Gordon, T.; Head-Gordon, M. From Intermolecular Interaction Energies and Observable Shifts to Component Contributions and Back Again: A Tale of Variational Energy Decomposition Analysis. *Annu. Rev. Phys. Chem.* **2021**, *72*, 641−666.
(27) Khaliullin, R. Z.; Cobar, E. A.; Lochan, R. C.; Bell, A. T.; Head-Gordon, M. Unravelling the Origin of Intermolecular Interactions Using Absolutely Localized Molecular Orbitals. *J. Phys. Chem. A* **2007**, *111*, 8753−8765.
(28) Horn, P. R.; Mao, Y.; Head-Gordon, M. Defining the Contributions of Permanent Electrostatics, Pauli Repulsion, and Dispersion in Density Functional Theory Calculations of Intermolecular Interaction Energies. *J. Chem. Phys.* **2016**, *144*, No. 114107.
(29) Horn, P. R.; Mao, Y.; Head-Gordon, M. Probing Non-Covalent Interactions with a Second Generation Energy Decomposition Analysis Using Absolutely Localized Molecular Orbitals. *Phys. Chem. Chem. Phys.* **2016**, *18*, 23067−23079.
(30) Mao, Y.; Levine, D. S.; Loipersberger, M.; Horn, P. R.; Head-Gordon, M. Probing Radical-Molecule Interactions with a Second

Generation Energy Decomposition Analysis of DFT Calculations Using Absolutely Localized Molecular Orbitals. *Phys. Chem. Chem. Phys.* **2020**, *22*, 12867−12885.
(31) Mao, Y.; Demerdash, O.; Head-Gordon, M.; Head-Gordon, T. Assessing Ion−Water Interactions in the AMOEBA Force Field Using Energy Decomposition Analysis of Electronic Structure Calculations. *J. Chem. Theory Comput.* **2016**, *12*, 5422−5437.
(32) Khaliullin, R. Z.; Bell, A. T.; Head-Gordon, M. Analysis of Charge Transfer Effects in Molecular Complexes Based on Absolutely Localized Molecular Orbitals. *J. Chem. Phys.* **2008**, *128*, No. 184112.
(33) Veccham, S. P.; Lee, J.; Mao, Y.; Horn, P. R.; Head-Gordon, M. A Non-Perturbative Pairwise-Additive Analysis of Charge Transfer Contributions to Intermolecular Interaction Energies. *Phys. Chem. Chem. Phys.* **2021**, *23*, 928−943.
(34) Shen, H.; Veccham, S. P.; Head-Gordon, M. Exactly Fragment Additive Breakdown of Polarization for Energy Decomposition Analysis Based on the Self-Consistent Field for Molecular Interactions. *J. Chem. Theory Comput.* **2023**, *19*, 8624−8638.
(35) Mayer, I. Charge, bond order and valence in the AB initio SCF theory. *Chem. Phys. Lett.* **1983**, *97*, 270−274.
(36) Mayer, I. Bond order and valence indices: A personal account. *J. Comput. Chem.* **2007**, *28*, 204−221.
(37) Ji, X.; Pei, Z.; Huynh, K. N.; Yang, J.; Pan, X.; Wang, B.; Mao, Y.; Shao, Y. On the entanglement of chromophore and solvent orbitals. *J. Chem. Phys.* **2025**, *162*, No. 064107.
(38) Ashcroft, N. W.; Mermin, N. D. *Solid State Physics*; Holt-Saunders, 1976.
(39) Larsen, A. H.; Mortensen, J. J.; Blomqvist, J.; Castelli, I. E.; Christensen, R.; Dułak, M.; Friis, J.; Groves, M. N.; Hammer, B.; Hargus, C.; Hermes, E. D.; Jennings, P. C.; Jensen, P. B.; Kermode, J.; Kitchin, J. R.; Kolsbjerg, E. L.; Kubal, J.; Kaasbjerg, K.; Steen, L.; Maronsson, J. B.; Maxson, T.; Olsen, T.; Pastewka, L.; Peterson, A.; Rostgaar, C.; Schiøtz, J.; Schütt, O.; Strange, M.; Thygesen, K. S.; Vegge, T.; Vilhelmsen, L.; Walter, M.; Zeng, Z.; Jacobsen, K. W. The atomic simulation environment—a Python library for working with atoms. *J. Phys.:Condens. Matter* **2017**, *29* (27), No. 273002.
(40) Kresse, G.; Hafner, J. Ab initio Molecular Dynamics for Liquid Metals. *Phys. Rev. B* **1993**, *47*, No. 558.
(41) Kresse, G.; Furthmüller, J. Efficiency of ab-initio Total Energy Calculations for Metals and Semiconductors Using a Plane-Wave Basis Set. *Comput. Mater. Sci.* **1996**, *6*, 15−50.
(42) Kresse, G.; Furthmüller, J. Efficient Iterative Schemes for ab initio Total-Energy Calculations Using a Plane-Wave Basis Set. *Phys. Rev. B* **1996**, *54*, No. 11169.
(43) Kresse, G.; Joubert, D. From Ultrasoft Pseudopotentials to the Projector Augmented-Wave Method. *Phys. Rev. B* **1999**, *59*, No. 1758.
(44) Monkhorst, H. J.; Pack, J. D. Special Points for Brillouin-Zone Integrations. *Phys. Rev. B* **1976**, *13*, No. 5188.
(45) Methfessel, M.; Paxton, A. T. High-Precision Sampling for Brillouin-Zone Integration in Metals. *Phys. Rev. B* **1989**, *40*, No. 3616.
(46) Pulay, P. Convergence Acceleration of Iterative Sequences. The Case of SCF Iteration. *Chem. Phys. Lett.* **1980**, *73*, 393−398.
(47) Press, W. H. *Numerical Recipes: The Art of Scientific Computing*; Cambridge University Press, 1986.
(48) Araujo, R. B.; Rodrigues, G. L. S.; Dos Santos, E. C.; Pettersson, L. G. M. Adsorption energies on transition metal surfaces: towards an accurate and balanced description. *Nat. Commun.* **2022**, *13*, No. 6853.
(49) Epifanovsky, E.; Gilbert, A. T. B.; Feng, X.; Lee, J.; Mao, Y.; Mardirossian, N.; Pokhilko, P.; White, A. F.; Coons, M. P.; Dempwolff, A. L.; Gan, Z.; Hait, D.; Horn, P. R.; Jacobson, L. D.; Kaliman, I.; Kussmann, J.; Lange, A. W.; Lao, K. U.; Levine, D. S.; Liu, J.; McKenzie, S. C.; Morrison, A. F.; Nanda, K. D.; Plasser, F.; Rehn, D. R.; Vidal, M. L.; You, Z.-Q.; Zhu, Y.; Alam, B.; Albrecht, B. J.; Aldossary, A.; Alguire, E.; Andersen, J. H.; Athavale, V.; Barton, D.; Begam, K.; Behn, A.; Bellonzi, N.; Bernard, Y. A.; Berquist, E. J.; Burton, H. G. A.; Carreras, A.; Carter-Fenk, K.; Chakraborty, R.; Chien, A. D.; Closser, K. D.; Cofer-Shabica, V.; Dasgupta, S.; de Wergifosse, M.; Deng, J.; Diedenhofen, M.; Do, H.; Ehlert, S.; Fang, P.-T.; Fatehi, S.; Feng, Q.; Friedhoff, T.; Gayvert, J.; Ge, Q.; Gidofalvi, G.; Goldey, M.; Gomes, J.; González-Espinoza, C. E.; Gulania, S.; Gunina, A. O.; Hanson-Heine, M. W. D.; Harbach, P. H. P.; Hauser, A.; Herbst, M. F.; Hernández Vera, M.; Hodecker, M.; Holden, Z. C.; Houck, S.; Huang, X.; Hui, K.; Huynh, B. C.; Ivanov, M.; Jász, Á.; Ji, H.; Jiang, H.; Kaduk, B.; Köhler, S.; Khistyaev, K.; Kim, J.; Kis, G.; Klunzinger, P.; Koczor-Benda, Z.; Koh, J. H.; Kosenkov, D.; Koulias, L.; Kowalczyk, T.; Krauter, C. M.; Kue, K.; Kunitsa, A.; Kus, T.; Ladjánszki, I.; Landau, A.; Lawler, K. V.; Lefrancois, D.; Lehtola, S.; Li, R. R.; Li, Y.-P.; Liang, J.; Liebenthal, M.; Lin, H.-H.; Lin, Y.-S.; Liu, F.; Liu, K.-Y.; Loipersberger, M.; Luenser, A.; Manjanath, A.; Manohar, P.; Mansoor, E.; Manzer, S. F.; Mao, S.-P.; Marenich, A. V.; Markovich, T.; Mason, S.; Maurer, S. A.; McLaughlin, P. F.; Menger, M. F. S. J.; Mewes, J.-M.; Mewes, S. A.; Morgante, P.; Mullinax, J. W.; Oosterbaan, K. J.; Paran, G.; Paul, A. C.; Paul, S. K.; Pavošević, F.; Pei, Z.; Prager, S.; Proynov, E. I.; Rák, Á.; Ramos-Cordoba, E.; Rana, B.; Rask, A. E.; Rettig, A.; Richard, R. M.; Rob, F.; Rossomme, E.; Scheele, T.; Scheurer, M.; Schneider, M.; Sergueev, N.; Sharada, S. M.; Skomorowski, W.; Small, D. W.; Stein, C. J.; Su, Y.-C.; Sundstrom, E. J.; Tao, Z.; Thirman, J.; Tornai, G. J.; Tsuchimochi, T.; Tubman, N. M.; Veccham, S. P.; Vydrov, O.; Wenzel, J.; Witte, J.; Yamada, A.; Yao, K.; Yeganeh, S.; Yost, S. R.; Zech, A.; Zhang, I. Y.; Zhang, X.; Zhang, Y.; Zuev, D.; Aspuru-Guzik, A.; Bell, A. T.; Besley, N. A.; Bravaya, K. B.; Brooks, B. R.; Casanova, D.; Chai, J.-D.; Coriani, S.; Cramer, C. J.; Cserey, G.; DePrince, A. E.; DiStasio, R. A.; Dreuw, A.; Dunietz, B. D.; Furlani, T. R.; Goddard, W. A.; Hammes-Schiffer, S.; Head-Gordon, T.; Hehre, W. J.; Hsu, C.-P.; Jagau, T.-C.; Jung, Y.; Klamt, A.; Kong, J.; Lambrecht, D. S.; Liang, W.; Mayhall, N. J.; McCurdy, C. W.; Neaton, J. B.; Ochsenfeld, C.; Parkhill, J. A.; Peverati, R.; Rassolov, V. A.; Shao, Y.; Slipchenko, L. V.; Stauch, T.; Steele, R. P.; Subotnik, J. E.; Thom, A. J. W.; Tkatchenko, A.; Truhlar, D. G.; Van Voorhis, T.; Wesolowski, T. A.; Whaley, K. B.; Woodcock, H. L.; Zimmerman, P. M.; Faraji, S.; Gill, P. M. W.; Head-Gordon, M.; Herbert, J. M.; Krylov, A. I. Software for the Frontiers of Quantum Chemistry: An Overview of Developments in the Q-Chem. 5 Package. *J. Chem. Phys.* **2021**, *155*, No. 084801.
(50) Andrae, D.; Häußermann, U.; Dolg, M.; Stoll, H.; Preuß, H. Energy-Adjusted ab initio Pseudopotentials for the Second and Third Row Transition Elements. *Theore. Chim. Acta* **1990**, *77*, 123−141.
(51) Weigend, F.; Ahlrichs, R. Balanced Basis Sets of Split Valence, Triple Zeta Valence and Quadruple Zeta Valence Quality for H to Rn: Design and Assessment of Accuracy. *Phys. Chem. Chem. Phys.* **2005**, *7*, 3297−3305.
(52) Boys, S.; Bernardi, F. The Calculation of Small Molecular Interactions by the Differences of Separate Total Energies. Some Procedures with Reduced Errors. *Mol. Phys.* **1970**, *19*, 553−566.
(53) Hopffgarten, M. v.; Frenking, G. Energy Decomposition Analysis. *WIRes: Comput. Mol. Sci.* **2012**, *2*, 43−62.
(54) Van Voorhis, T.; Head-Gordon, M. A Geometric Approach to Direct Minimization. *Mol. Phys.* **2002**, *100*, 1713−1721.
(55) Perdew, J. P.; Burke, K.; Ernzerhof, M. Generalized Gradient Approximation Made Simple. *Phys. Rev. Lett.* **1996**, *77*, No. 3865.
(56) Grimme, S.; Antony, J.; Ehrlich, S.; Krieg, H. A Consistent and Accurate *ab initio* Parametrization of Density Functional Dispersion Correction (DFT-D) for the 94 Elements H-Pu. *J. Chem. Phys.* **2010**, *132*, No. 154104.
(57) Grimme, S.; Ehrlich, S.; Goerigk, L. Effect of the Damping Function in Dispersion Corrected Density Functional Theory. *J. Comput. Chem.* **2011**, *32*, 1456−1465.
(58) Hammer, B.; Hansen, L. B.; Nørskov, J. K. Improved Adsorption Energetics Within Density-Functional Theory Using Revised Perdew-Burke-Ernzerhof Functionals. *Phys. Rev. B* **1999**, *59*, No. 7413.
(59) Adamo, C.; Barone, V. Toward reliable density functional methods without adjustable parameters: The PBE0 model. *J. Chem. Phys.* **1999**, *110*, 6158−6170.
(60) Krukau, A. V.; Vydrov, O. A.; Izmaylov, A. F.; Scuseria, G. E. Influence of the exchange screening parameter on the performance of screened hybrid functionals. *J. Chem. Phys.* **2006**, *125*, No. 224106.

https://doi.org/10.1021/jacsau.5c00111
JACS Au 2025, 5, 3092−3103

(61) Henderson, T. M.; Janesko, B. G.; Scuseria, G. E. Generalized gradient approximation model exchange holes for range-separated hybrids. *J. Chem. Phys.* **2008**, *128*, No. 194105.
(62) Hermann, K.; Bagus, P. S.; Nelin, C. J. Size Dependence of Surface Cluster Models: CO Adsorbed on Cu(100). *Phys. Rev. B* **1987**, *35*, No. 9467.
(63) Stone, A. *The Theory of Intermolecular Forces*; Oxford Univ. Press, 2013.
(64) Mao, Y.; Horn, P. R.; Head-Gordon, M. Energy Decomposition Analysis in an Adiabatic Picture. *Phys. Chem. Chem. Phys.* **2017**, *19*, 5944−5958.
(65) Anderson, P. W. Localized Magnetic States in Metals. *Phys. Rev.* **1961**, *124*, No. 41.
(66) Newns, D. M. Self-Consistent Model of Hydrogen Chemisorption. *Phys. Rev.* **1969**, *178*, No. 1123.
(67) Grimley, T. B. Overlap Effects in the Theory of Adsorption Using Anderson's Hamiltonian. *J. Phys. C* **1970**, *3*, 1934−1942.
(68) Norsko, J. K. Chemisorption on Metal Surfaces. *Rep. Prog. Phys.* **1990**, *53*, 1253−1295.
(69) Larsen, A. H.; Kleis, J.; Thygesen, K. S.; Nørskov, J. K.; Jacobsen, K. W. Electronic Shell Structure and Chemisorption on Gold Nanoparticles. *Phys. Rev. B* **2011**, *84*, No. 245429.
(70) Vijay, S.; Kastlunger, G.; Chan, K.; Nørskov, J. K. Limits to Scaling Relations Between Adsorption Energies? *J. Chem. Phys.* **2022**, *156*, No. 231102.
(71) Kakekhani, A.; Roling, L. T.; Kulkarni, A.; Latimer, A. A.; Abroshan, H.; Schumann, J.; AlJama, H.; Siahrostami, S.; Ismail-Beigi, S.; Abild-Pedersen, F.; Nørskov, J. K. Nature of Lone-Pair−Surface Bonds and Their Scaling Relations. *Inorg. Chem.* **2018**, *57*, 7222−7238.
(72) Zare, M.; Sahsah, D.; Saleheen, M.; Behler, J.; Heyden, A. Hybrid Quantum Mechanical, Molecular Mechanical, and Machine Learning Potential for Computing Aqueous-Phase Adsorption Free Energies on Metal Surfaces. *J. Chem. Theory Comput.* **2024**, *20*, 8247−8260.
(73) Mandal, A.; Taylor, M. A.; Weight, B. M.; Koessler, E. R.; Li, X.; Huo, P. Theoretical Advances in Polariton Chemistry and Molecular Cavity Quantum Electrodynamics. *Chem. Rev.* **2023**, *123*, 9786−9879.

https://doi.org/10.1021/jacsau.5c00111
JACS Au 2025, 5, 3092−3103